On the Actuator Requirements for Human-Like Execution of Retargeted Human Motion on Humanoid Robots

Cornelius Klas, Andre Meixner, Daniel Ruffler and Tamim Asfour

***Abstract*— Building humanoid robots with properties similar to those of humans in terms of strength, agility, and motion versatility remains a challenge. To achieve human-like motion behavior, an identification of the actuation requirements is crucial. In this paper, we propose a novel approach that automatically calculates the necessary actuator requirements for a given upper-body humanoid robot kinematics performing motions retargeted from human motion data. First, we introduce a unified representation of humanoid upper limb kinematics to decouple the analysis from robot-specific features to allow the comparison between different humanoid robot kinematics. Second, we derive a novel performance index to compare actuator requirements regarding velocity, acceleration, and torque for different kinematics, which are needed for the execution of retargeted human motions. We evaluate our approach by comparing the calculated actuator requirements and performance indices of ten existing humanoid robot kinematics in addition to a new robot design, using 40 recorded human motions of different categories. The results demonstrate the impact of robot kinematics on the joint actuator requirements for achieving human-like motion.**

I. Introduction

Humanoid kinematics and human-like motion trajectories and velocities are desired for intuitive human-robot interaction and collaboration in environments created for humans. Previous work on the design and maintenance of our ARMAR robots ([1], [2], [3]) and in analyzing other robots (e. g. [4], [5], [6], [7]) has shown that building humanoids with properties similar to those of humans in terms of force and agility remains, despite advances in actuator and sensor technology, a major challenge. Humanoid robots have been designed to perform tasks in different environments, however, less attention has been put on the actuation and kinematics requirements needed for achieving natural human-like motion of these robots. To do so, it is important to consider the execution of human-like motions [8] already in the robot design process and not only during motion generation. While considerable work and knowledge exist regarding the identification of actuator requirements for human-like walking motions e. g. , based on the analysis of the gait cycle [9], such requirements for a versatile set of upper-body motions are still missing. Even if human joint actuation torques and velocities are known, they first need to be transferred to the corresponding robot arm kinematics. In this work, we propose a system that can automatically calculate actuator requirements regarding velocity, acceleration, and torque for different robot kinematics based on human motions.

This work has been supported by the Carl Zeiss Foundation through the JuBot project.

The authors are with the High Performance Humanoid Technologies Lab, Institute for Anthropomatics and Robotics, Karlsruhe Institute of Technology (KIT), Germany {klas, meixner, asfour}@kit.edu

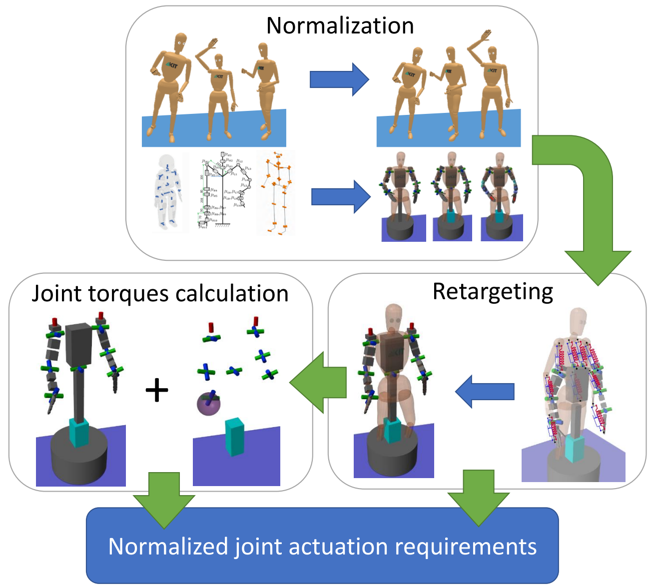

Fig. 1: Joint actuation requirement calculation: 1. Normalization, 2. Virtual spring-damper systems for motion retargeting, 3. calculation of the robot joint torques with robot segment weights and with object weights.

In our previous work, we introduced the Master Motor Map (MMM) framework[1] [10], which unifies the representation of human motion by decoupling the human motion capture process from further post-processing tasks such as motion analysis, retargeting and reproduction on a robot. At its core, the MMM encompasses a reference model of the human body with kinematic (joints and segment lengths) and dynamic (segment mass, center of mass, and moments of inertia) properties. In addition, the MMM defines an anthropomorphic model, by which segment properties (e. g. , length, mass etc.) are defined as a function with global body parameters (e. g. , body height and weight). The parameters of the MMM reference model are derived from the biomechanics literature and motion recording studies. Based on the MMM reference model, motion data captured by different subjects and by different motion capture systems can be normalized uniformly to the MMM human reference body model. In this work, we first extend the concept of this unified representation of the human body and motion to a unified representation of humanoid robot kinematics. To this end, we normalize different humanoid kinematics and

[1] https://git.h2t.iar.kit.edu/sw/mmm

provide model laws to scale human motion with respect to a normalized MMM reference model (section III-A). In order to develop and evaluate our approach for identifying actuator requirements for human-like motions, we retarget motions of uni- and bimanual human demonstrations to the normalized robot kinematics to compute joint positions, velocities and accelerations (section III-B), as well as joint torques using the normalized dynamic properties of the MMM reference model (section III-C). On this basis, we compute the normalized or actual minimum actuator requirements for performing such human motions on a certain humanoid kinematics (section III-D).

Contribution: *(i)* We develop a method to calculate actuation requirements for a humanoid robot kinematics based on a set of human motions; *(ii)* We derive a novel *performance index* based on normalized required actuator power for retargeted human motions to compare different humanoid kinematics. We show that our system allows us to evaluate the actuator requirements for various upper-body humanoid kinematics of different humanoid robots – as seen in Figure 7 – to perform human-like motion trajectories based on the retargeting of human motions taken from the KIT Whole-Body Human Motion Database[2] [11]. We demonstrate that we can take advantage of our novel framework in order to evaluate a new design for humanoid robot arms based entirely on quaternion joints [12], [13].

II. Related Work

We provide an overview on the state of the art regarding motion retargeting and robot kinematics comparison.

A. Motion Retargeting

Joint actuation requirements based on human motion are rarely available for arm motions, especially for different humanoid kinematics. In order to obtain actuator requirements for humanoid robots based on the execution of human-like motions, recorded human demonstrations must first be retargeted to the different robot kinematics. A general problem with the transfer of human poses is that there is no single solution for solving the inverse kinematics of multi-joint movements due to the high redundancy in the human body. In addition, not all end-effector positions can be achieved for full-body poses, and not all robot segments can be in the same position as the human counterpart if the segment lengths are different. Various methods, optimizations and constraints have been used in the literature to solve this motion retargeting problem.

If the robot kinematics are very similar to human kinematics, analytical solutions can be used for motion imitation [14]. The same applies when exact end-effector poses are not important, allowing direct mapping of joint angles.

The joint angles for the robot can be directly calculated from the kinematic model of the human. In most cases, however, the end-effector poses are relevant because the difference from human to robot kinematics is too large to ignore, and other constraints such as singularities have to be considered. Various approaches based on inverse [15] or forward kinematics with non-linear optimization, e. g., quadratic programming [16], can be used to match the end-effector pose while taking additional constraints such as manipulability tracking, temporal smoothness or joint limits into account. A disadvantage is that this requires a mathematical description of forward or inverse kinematics. Other approaches use for example convolutional neural networks [17], reinforcement learning [18] or unsupervised learning [19]. However, there is no guarantee that learning-based solutions can be applied to completely new robot kinematics in the intended manner.

A different solution for multi-joint reaching motions with a spring-damper system is proposed in [20]. Thereby, a virtual spring-damper hypothesis is used to pull the endpoint to the target. This leads to a simple structure of the control signals without solving the inverse kinematics or the inverse dynamics, and without planning an endpoint trajectory. However, this method is dependent on proper initial poses.

In this work, we use a method similar to the virtual spring-damper system of [20] in order to cover a wide variety of different joint kinematics. Classical inverse kinematics solvers provide support for a fixed set of joint types while we can compose complex joints like parallel and cable driven mechanisms from Simulink elements. Therefore, this approach enables new kinematics, e.g., quaternion joints, to be added in a very simple way, without the need for a mathematical description of the forward kinematics to quickly evaluate new designs. We add multiple virtual spring-damper systems with variable stiffness to achieve high similarity with the reference human demonstration and ensure human-like motions.

B. Kinematics Comparison

When reviewing and comparing different robot kinematics, a *performance index* [21] to quickly evaluate one kinematic design against another is needed. This can be done either based on general criteria or application- or task-based.

General metrics are reachability and manipulability analyses. The reachability distribution, a workspace representation of the robot's capabilities for the search of suitable robot base poses [22], can also be used to compare different kinematics. Manipulability ellipsoids [23] indicate the favored directions of force or velocity at a given joint configuration. Various indices can be computed for voxels in the robot's workspace to obtain a distribution of manipulability. The Yoshikawa manipulability index [23] is based on the volume of the manipulability ellipsoid, while the extended manipulability measure [24] includes additional constraints. The condition number of the Jacobian Matrix [25] is used as a measure of kinematic accuracy as well as proximity to singularity.

Previous studies related to application-based performance indices use very different approaches. For the evaluation of humanoid hands, an index is presented in [26] that counts the intersection volume of the working space of the fingertips.

[2]https://motion-database.humanoids.kit.edu

If the desired manipulability ellipsoids for a task are known, the closeness between the desired and actual manipulability ellipsoids yields the task-specific quality function for a redundant manipulator [27]. To match the desired manipulability ellipsoids from human demonstration, a manipulability transfer framework is presented in [28] to learn and reproduce manipulabilities for robot kinematics.

In evolutionary robotics (ER), robots perform a competition in a specific task in each evolution cycle to evaluate fitness. The sensory apparatus, the morphology, and the control of the robot evolve simultaneously in this process. In [29], the fitness of simulated soft robots consisting of different types of voxels is calculated based on the distance traveled in four environments. The kinematic design, e. g. , of a manipulator [30], can also simultaneously evolve to perform task-specific object manipulations in physics simulation based on the distance to a given reference object trajectory. In ER, this *performance index* can also be environment-driven [31] rather than manually selected. Simulating the morphology and control to complete specific tasks with targeting real robots is challenging, and therefore this type of quality measurement is only performed for a small number of limited tasks in simplified environments.

Since the desired robots should work in human environments with made-for-human tools, it is desirable to include this in the assessment. One metric applied in motion retargeting that could also be adopted for kinematic comparison is the quantification of human likeness. These metrics for functional anthropomorphism can be Cartesian joint distance, similarity of the convex hull, as well as the area of the triangles between individual joints [32]. Other metrics are for example spatial and temporal correspondences [33] or comfort and effort of the human [34].

We propose a novel *performance index* based on actuator requirements for retargeted human motion. The actuator weight and size is approximately proportional to its maximum power, and the reduced arm weight further reduces the required actuator power. This could have a large impact on achieving human-like motion. To our best knowledge, no other existing approaches provide a kinematics *performance index* based on retargeted human motion.

III. Approach

The desired system should automatically calculate the necessary actuator requirements for a given robot kinematic to perform selected human motions. A general anthropomorphic kinematics, segment length, and weight distribution of the robots are required to produce meaningful results.

A. Normalization

In the MMM framework [10], a human demonstration is mapped to the MMM reference model of the human body, which is scaled by height and weight of the corresponding subject. In order to map this subject-specific motion to a differently scaled or to the normalized MMM model, the execution speed of the motion has to be adjusted to account for changes in the dynamic properties. Therefore, we extend the conversion between kinematics in the MMM framework to allow adapting the motion to be executed not only by the MMM human body reference model but also by a general robot kinematics. This allows the calculation of dynamics on normalized models for uniform comparison of kinematic designs and their transfer to robots of arbitrary size and weight without recalculation.

The required equations for scaling, called model or similarity laws, can be derived from dimensional analysis [35]. The approach originates from fluid mechanics, where data from machines of different types and sizes is compared. For the scaling of humans and robots, the characteristic key figure is the Froude number $Fr = \frac{v^2}{g \cdot l} = \frac{l}{g \cdot t^2}$, which is given by the ratio of the inertial force to the force of gravity.

With the scaling factors for length $\lambda = l_{source}/l_{target}$ and mass $\mu = m_{source}/m_{target}$ (and constant g), the scaling laws for time t (Eq. 2), force F (Eq. 3), torque τ (Eq. 4), and power P (Eq. 5) can be derived.

$$Fr_{source} = Fr_{target} \Rightarrow \frac{l_{source}}{t^2_{source}} = \frac{l_{target}}{t^2_{target}} \; [\tfrac{L}{T^2}] \quad (1)$$

$$\Rightarrow \lambda = \frac{t^2_{source}}{t^2_{target}} \Rightarrow t_{target} = \frac{1}{\sqrt{\lambda}} \cdot t_{source} \; [\mathrm{T}] \quad (2)$$

$$F_{target} = \frac{1}{\mu} \cdot F_{source} \qquad [\tfrac{M \cdot L^2}{T^2}] \quad (3)$$

$$\tau_{target} = \frac{1}{\mu \cdot \lambda} \cdot \tau_{source} \qquad [\tfrac{M \cdot L^2}{T^2}] \quad (4)$$

$$P_{target} = \frac{1}{\mu \cdot \sqrt{\lambda}} \cdot P_{source} \qquad [\tfrac{M \cdot L^2}{T^3}] \quad (5)$$

In our new representation, the robot kinematics are based on their real counterpart regarding segment length, transformations between joints, and joint type. The size is scaled to match the $1\,\mathrm{m}$ MMM model arm lengths (torso center to hand, with arms extended to the side in $45\,\mathrm{deg}$ angle). Joint limits are only considered if they change the desired kinematic behavior (e. g. change direction of elbow shift). To standardize the segment weights of the robot arms for comparability, we set the individual segment weights of the robot to match the MMM reference model [10] scaled to $100\,\mathrm{kg}$. This leads to a total weight of $8\,\mathrm{kg}$ per arm.

The described formulas are first used for mapping human motions from the subject-specific to the normalized MMM reference model described above. Via motion retargeting in section III-B, the motions are then also transferred to the normalized robot kinematics model. A transfer using the same formulas can be applied to transfer the motions from the normalized robot to real robots of arbitrary size and weight to obtain the actual joint requirements (section III-D). The applicability of the developed scaling laws was tested with a simplified simulation (Figure 2). Normalized human joint motion was executed on different 1 DoF arms of different size. The normalized joint parameters (e. g. , joint torque and joint power) should be equal as can be seen in

Figure 2. The change in arm thickness for the same length, which occurs in humans and robots, is not covered by the scaling laws, but has a negligible influence on the results.

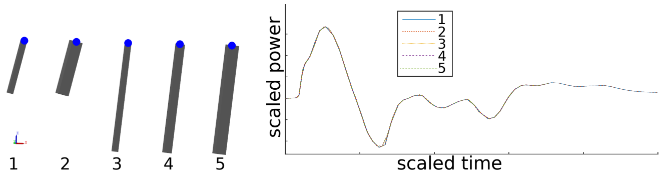

(a) Actuated bars (b) Joint power

Fig. 2: Validation of scaling with model laws. Different bars with constant density are actuated at a joint (●) with a normalized trajectory. Length and weight difference is compensated by normalization leading to nearly identical curves. Different thickness lead to a small systematic error of maximum 4%.

For a unified representation of the different robot kinematics, we use the description of kinematics illustrated in Figure 3. Based on this description, a new robot kinematics can be added to the system with the following parameters: the joint types (Figure 4) in the joint centers j_1 to j_3, and the activation of the rotational joints jC and jR_0 to jR_3. The transformations T_C and T_0 to T_3 describe the segment lengths as well as rotations and offsets of the joints. Since the focus of this work is on the upper-body motion, the movement of the torso is modeled as a holonomic platform, where additional DoF can be activated in the hip.

B. Human Motion Retargeting

The motions selected as input must be normalized MMM motions. From the various motions in the KIT Whole-Body Human Motion Database [11], a set representing the desired robot task must be selected. Motion retargeting, aimed at closely resembling human motions, is performed with a virtual spring-damper system. The method ([20]) of hand positioning is extended by approximating also the torso, shoulder, and elbow positions by Cartesian spring damper systems as seen in the retargeting step in Figure 1. The hand orientation is directly taken from the MMM hand orientation. The springs in the hand are much stiffer to prioritize the hand position over the others, since it is more important for most task executions. Stiffnesses and damping must be chosen to achieve a balance between smoothness, accuracy, and oscillations, with acceptable results for a wide range of values. The effects close to singularities are reduced by the inertia of the robot arm segments, which limit possible accelerations. Gravity is not considered during retargeting to avoid a constant error in the gravity direction. The retargeting system is calculated with ode45, the MATLAB Simulink implementation of a variable-step continuous explicit solver. From the transfer of the motions, the positions, velocities and accelerations for all joints are obtained.

C. Calculation of Joint Torques

The joint motions obtained from motion retargeting are executed on normalized robot models. The joint torques are obtained by numerical calculation of multi-body dynamics in

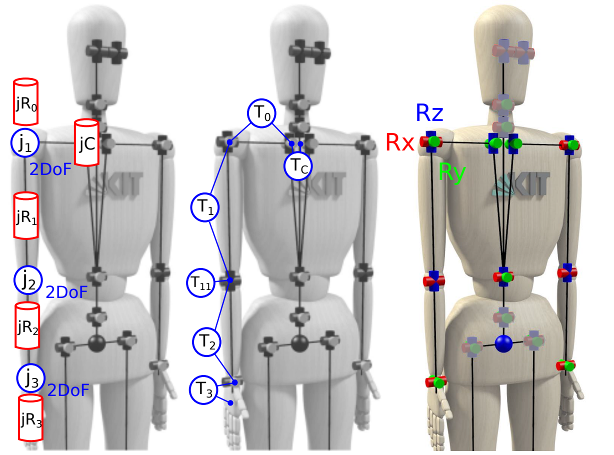

Fig. 3: Kinematics of humanoid robots used in this work. Different joints (left) and transformations (middle) can be specified. Axis directions (right) based on MMM [10] model.

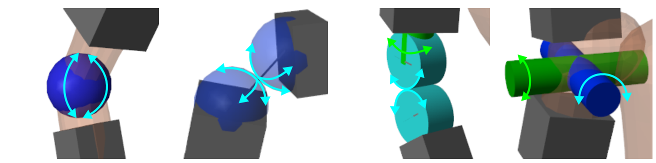

(a) cv (2 DoF) (b) quat (2 DoF) (c) roll (2 DoF) (d) xy (2 DoF)

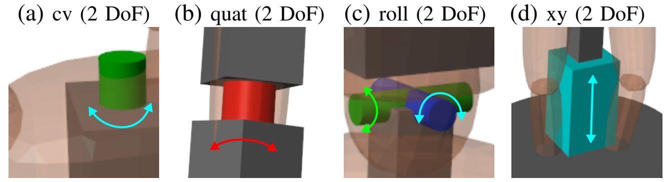

(e) jC (f) jR0 to jR3 (g) Torso Rx,y (h) Torso Pz

Fig. 4: Joint types for kinematics in Table I: Const. velocity joint (cv), quaternion joint (quat), Rz and rolling contact (roll), universal joint (xy, xz), clavicula joint (jC), arm rotation (jR0 to jR3), rotary torso joints (Rx, Ry) and prismatic torso joint (Pz).

MATLAB Simulink. In order to acquire comparable dynamic models from the kinematic models, inertia corresponding to those of the MMM model are added to the corresponding robot segment positions. The calculation is separated into robot joint torques with segment weights and with object weights (Figure 1). The following combination allows separate scaling of object and robot weights.

The accuracy of the numerical torque calculation was validated with a grasping motion recorded on our humanoid robot ARMAR-6. The recorded joint trajectory was used and the calculated torque was compared to the measured one. The result is shown in Figure 5. At the end of the grasping motion, the robot configuration is close to a singularity, which causes oscillations that can not be reproduced in rigid body dynamics. This must be considered when selecting actuators based on the calculated requirements. The mean error between measured and computed torque is 1.8%.

D. Actuator Requirements and Performance Index

The actuator requirements regarding velocity and acceleration are obtained from motion retargeting, the torque requirements from the normalized dynamic robot model. To

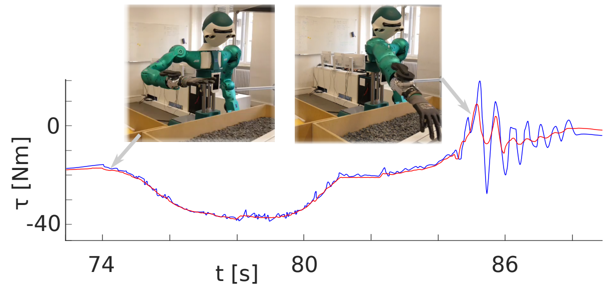

Fig. 5: Measured torque (—), and numerically calculated torque (—) of the first right shoulder joint (j_{1a}) of ARMAR-6 during grasping motion.

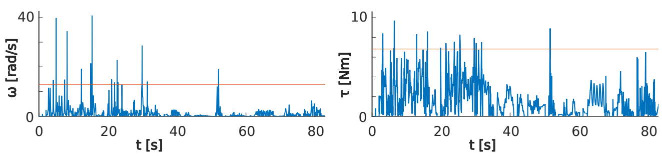

(a) Joint velocity.

(b) Joint torque.

Fig. 6: Temporal trajectory of velocity and torque (—) in the LIMS2 kinematics j1a joint together with the 99th percentile value (—) used in robot comparison.

limit the influence of short peaks in the motions, each value is limited to the 99th percentile of the values (see Figure 6). Then, the power requirements for each actuator are calculated by the multiplication of torque and velocity. The specified motions lead to asymmetrical loads in the left and right arm. Due to symmetry considerations, the maximum of both arms is used.

For the simple comparison of different kinematics, a *performance index* based on required normalized actuator power is proposed. The joint power results from the product of joint speed ($j_{n\omega}$) and torque ($j_{n\tau}$). The index is based on the combined actuator power in one arm, where N is the number of joints in one arm:

$$P = \sum_{n=0}^{N} j_{n\omega} \cdot j_{n\tau} \tag{6}$$

The *Power Requirement Index* (PRI) is then the ratio of the required actuation power of the robot to the reference model.

$$PRI = \frac{P_{robot}}{P_{MMM}} \tag{7}$$

Since the actuator's weight and size is approximately proportional to its maximum power, this is a meaningful value. Lower values mean that less power is required for the same motion and are therefore better.

IV. Requirements Analysis

In the following, we identify the requirements for different dynamic, human-like uni- and bimanual manipulation movements for different robotic kinematics. For their comparison, we apply the proposed *performance index*.

A. Robot Kinematics

10 different humanoid robot kinematics (see Table I, Figure 4 and Figure 7) are chosen for comparison: *LIMS2* [36], *CENTAURO* [37], *iCub* [38], *David* [4], *Justin* [5], *HRP-4* [6], *Valkyrie* [7], *ARMAR-III* [1], *ARMAR-4* [2] and *ARMAR-6* [3]. We have chosen a diverse set of humanoid robot kinematics with 7 or more DoF per arm. Humanoid kinematics with all joints in a straight line ([6], [7]), are accompanied with kinematics with a very long wrist ([37]), different shoulder rotations ([37], [38], [3], [4], [5]), and with different elbow displacements ([1], [2], [3]). Additional kinematics with special joint types ([36], [4]) were also selected. Next to the kinematics of existing humanoid robots, we also added a *New Design* based on quaternion joints [13] in all 3 joint centers. Quaternion joints offer advantages like a large singularity-free range of motion and high manipulability across their spherical motion pattern. They could also lead to a more human-like movement of the robot arm: Although human joints are often modeled by rotary joints, this does not accurately mimic the human joint motion. This design was not optimized against the *PRI* before. Finally, the kinematic design *MMM* is used for comparison. The MMM kinematic has no mechanical realization yet, and the joint positions and orientations are taken directly from the MMM model.

TABLE I: Specifications of Robot Kinematic Examples

	jR	j1	j2	j3	Torso *	λ	δ **
LIMS2 [36]	jR3	xy	roll	quat	Pz	0.48	7%
CENTAURO [37]	jR1	xy	xz	xz	Rx,Ry,Pz	0.40	22%
iCub [39]	jR1	xy	xz	xy	Rx,Ry,Pz	0.95	4%
David [4]	jR1	xy	xz	quat	Rx,Ry	0.39	15%
Justin [5]	jR2	xy	zx	xy	Rx,Pz	0.33	20%
HRP-4 [6]	jR2	xy	zx	xy	Rx,Ry,Pz	0.58	6%
Valkyrie [7]	jR2	xy	zx	yx	Rx,Ry,Pz	0.44	2%
ARMAR-III [1]	jR1	xy	xz	xy	-	0.43	5%
ARMAR-4 [2]	jRC, jR1	xy	xz	xy	Rx,Ry,Pz	0.50	5%
ARMAR-6 [3]	jRC, jR1	xy	xz	xy	Pz	0.31	11%
New Design	jR3	quat	quat	quat	Rx,Ry,Pz	0.47	9%
MMM [10]	jR0	xy	xy	xy	Rx,Ry,Pz	1.00	0%

* A holonomic platform is added to all kinematics
** δ: Sum of segment length deviation from MMM related to arm length

The abbreviations for joint centers (jC, jR, j1, j2, j3, Torso) refer to Figure 3. Additional z-axis rotation is available at 5 positions on the arm. The directions (x, y, z) refer to the MMM model. The 2d joint types are the following: universal joints with different axis (xy, xz), 1d rolling contact joint combined with a orthogonal rotation (roll), 2d rolling contact joint, also called quaternion joint (quat), and a constant velocity joint (cv) defining azimuth and elevation. The 1 DoF arm joints (clavicula joint (jR) and arm torsion joints (jR_0 to jR_3)) are always revolute joints around the z-axis. Based on this system and the transformations between the joints, most humanoid robot arms with 6-8 degrees of freedom can be constructed in the written Simulink program with one line of text describing the parameters. The base is connected to the world with a planar joint, enabling the motion of a holonomic platform. The possible joints following are a prismatic joint in z-direction (Pz) and revolute joints (Rx,Ry).

B. Human Motion Retargeting

40 motions from the KIT Whole-Body Human Motion Database [11] were selected and categorized into the following 4 categories: Household H, Entertainment E, Conversation C and Factory F. The first two categories have

Fig. 7: Rendering of a unified representation of 9 humanoid robots with different kinematics performing a retargeted Conversation motion.

TABLE II: Specifications of Selected Motions

	Household	Entertainment	Factory	Conversation
#	586 01	207 05	529 01	323 03
Object	0.3 kg	0 kg	0.3 kg	0 kg
Descr.	Big sponge	Drum	Pick & place	Point at left
#	589 01	316 01	663 02	323 03
Object	1 kg	0 kg	biman. 4 kg	0 kg
Descr.	Pour	Air guitar	Cast box	Point at right
#	589 03	636 15	1071 70 09	597 01
Object	0.5 kg	0 kg	5 kg	0 kg
Descr.	Pour & mix	Guitar right	Suitcase	Lean over
#	944	638 16	1758 1p25 01	597 07
Object	0.5 kg	0 kg	biman. 1.25 kg	0 kg
Descr.	Put in bowl	Violin right	Manipulate	Lean over
#	1235 04	651 01	1758 2p5 01	660 01
Object	0.5 kg	0 kg	biman. 2.5 kg	0 kg
Descr.	Book f. shelf	Head and sh.	Manipulate	Gestures
#	1235 05	995 131 01	1758 5 01	660 02
Object	0.5 kg	0 kg	biman. 5 kg	0 kg
Descr.	Book f. shelf	M. J. dance	Manipulate	Gestures
#	1259 46	1109 94 06	1759 1p25 01	1268 01
Object	0.5 kg	0 kg	biman. 1.25 kg	0 kg
Descr.	Hand over	Indian dance	Manipulate	Control table
#	1269 02	1109 94 07	1759 2p5 01	1268 05
Object	0.1 kg	0 kg	bim. 2.5 kg	0 kg
Descr.	Throw left	Indian dance	Manipulate	Control table
#	1283 01	1258 36	1759 5 01	1327 01
Object	0.1 kg	0 kg	biman. 5 kg	0 kg
Descr.	Throw right	Circular	Manipulate	Wave both
#	1071 70 09	1288 05	1759	634 01
Object	0.1 kg	0 kg	biman. 4 kg	0 kg
Descr.	Carry & lift	Left punch	Manipulate	Left wave

no additional weight at the hand, while the latter two add objects to the hand with weights appropriate to the task. The details of the categories can be found in Table II. These motions from the database are already mapped onto the subject-specific MMM reference model. The normalization and retargeting is working on all selected robot kinematics. To evaluate the chosen motion retargeting method, the mean error between the motion on the normalized MMM reference model and the retargeted motion on each robot kinematic is computed. The results are shown in Table III.

TABLE III: Mean retargeting errors separately for end-effector and other joints for the four motion categories

	Δ shoulder & elbow [mm]				Δ hand [mm]			
	H	E	F	C	H	E	F	C
LIMS2	25.0	24.8	25.3	22.9	2.0	2.0	1.7	1.9
CENTAURO	30.5	34.3	28.5	31.3	1.5	3.3	1.1	1.7
iCub	9.8	10.8	9.5	10.7	0.9	1.6	0.6	1.1
David	40.6	43.0	40.5	39.1	2.8	3.6	2.4	3.3
HRP-4	10.7	12.7	10.4	11.1	0.6	1.4	0.5	0.7
Justin	33.1	35.3	30.6	32.4	2.1	2.7	1.8	2.0
Valkyrie	3.4	4.1	3.2	3.3	0.4	1.1	0.4	0.4
ARMAR-III	29.8	37.8	41.4	21.4	2.4	8.9	11.9	1.5
ARMAR-4	10.6	11.2	10.1	11.0	1.0	1.5	0.9	1.2
ARMAR-6	20.4	19.4	16.8	18.2	1.8	2.0	1.4	1.7
New Design	15.1	16.2	14.9	15.5	0.9	1.5	0.9	1.0
MMM	1.0	2.3	0.9	0.6	0.3	1.1	0.3	0.4

C. Analysis

The actuation requirements of velocity, torque and acceleration, the derived actuation power and proposed *performance index* PRI were calculated for all combinations. The normalized results are plotted in Figure 8 with their maximum values in Table IV. All Units refer to $1\,\mathrm{m}$ and $100\,\mathrm{kg}$ scale. The abbreviations for joint based power requirement (jC, jR, j1a, j2a, j3a, j1b, j2b, j3b) refer to the joint names in Figure 4. For 2 DoF joints, the two degrees of freedom *a* and *b* are added for the two part joints. The computed power requirements and PRI are shown in Table V.

In all motion categories, the best kinematics requires only about 40% of the drive power of the worst kinematics, indicating the high importance of selecting suitable kinematics. Most kinematics perform similarly in the different motion categories. Some kinematics perform best in only one category (Valkyrie in Factory) or require the highest drive power in only one category (ARMAR-III in Factory). The various requirements for each joint such as velocity and torque are either all high (e. g. CENTAURO) or all low (e. g. Justin) for a kinematic. However, certain kinematics (New Design, LIMS2, David) have increased torque but reduced velocity requirements in some joints which can be explained by the transmission characteristics of rolling contact (quat) joints. In general, the reasons for the performance of the various robot kinematics and ways to improve them require further investigation. Overall, the proposed analysis and computed PRI (see Table V) shows that the new kinematic design performs best in 3 categories and well in the last category. However, its mechanical implementation is challenging.

V. Discussion

This paper presented a system that automatically calculates the actuator requirements for humanoid robot arms based on retargeted human motion. It can be seen that the pipeline for transferring human-like motion trajectories is suitable for various bimanual humanoid arm kinematics. Our system allows us to calculate the normalized joint torques, velocities, and accelerations (Figure 7) for all arm joints. We show that

Fig. 8: Normalized velocity (—), acceleration (—) and torque (—) of all arm joints in corresponding order (jC, jR, j1a, j1b, j2a, j2b, j3a, j3b) for 12 different kinematics and the four motion categories. Complete arm actuator power requirement in background ( ). The values are normalized with the maximum of all robots for each respective joint. The individual scaling factors (maximum values) are given in Table IV.

TABLE IV: Maximum values of velocity, acceleration and torque for all joints and the four motion categories

	H	E	F	C
$jC_\omega[rad/s]$	1.53	3.24	1.29	2.24
$jC_\alpha[rad/s^2]$	54.2	127.1	92.8	417.9
$jC_\tau[Nm]$	7.60	11.79	12.72	8.11
$jR_\omega[rad/s]$	10.38	23.99	11.33	6.90
$jR_\alpha[rad/s^2]$	184.7	692.5	207.1	377.9
$jR_\tau[Nm]$	2.85	5.08	4.77	2.49
$j1a_\omega[rad/s]$	8.71	24.21	5.28	6.19
$j1a_\alpha[rad/s^2]$	158.0	673.4	181.6	540.7
$j1a_\tau[Nm]$	7.50	10.87	10.15	6.72
$j2a_\omega[rad/s]$	7.30	21.54	5.54	7.76
$j2a_\alpha[rad/s^2]$	258.2	850.0	456.7	904.3
$j2a_\tau[Nm]$	5.68	9.20	11.64	8.07
$j3a_\omega[rad/s]$	5.55	11.58	3.36	4.26
$j3a_\alpha[rad/s^2]$	148.0	394.7	179.2	379.1
$j3a_\tau[Nm]$	1.88	2.01	4.47	1.33
$j1b_\omega[rad/s]$	6.15	9.60	3.21	5.17
$j1b_\alpha[rad/s^2]$	70.9	231.4	85.5	221.5
$j1b_\tau[Nm]$	13.33	19.78	15.20	13.54
$j2b_\omega[rad/s]$	16.33	30.98	12.59	15.03
$j2b_\alpha[rad/s^2]$	310.2	952.9	227.3	588.3
$j2b_\tau[Nm]$	5.86	8.22	11.74	4.65
$j3b_\omega[rad/s]$	13.02	31.42	11.71	14.65
$j3b_\alpha[rad/s^2]$	307.5	962.0	265.0	685.7
$j3b_\tau[Nm]$	1.57	2.68	3.91	1.35

it is possible to perform human-like motion trajectories based on the retargeting of human motions available in the KIT Whole-Body Human Motion Database.

We demonstrate that we can take advantage of our novel framework in order to evaluate existing kinematics and a new design. The speed, acceleration, and torque requirements (Figure 8 and Table IV) can serve as a basis for dimensioning the joint actuation in future robotic systems. The *Power Requirement Index* (PRI), a new *performance index*, was introduced and applied to the new design based on general considerations for improving robot dynamics. With the new index, these considerations could be confirmed and the effect quantified (Table V). We showed that under the chosen assumptions of a constant segment weight distribution, the kinematic structure of the robot has a significant impact on the required joint actuation power. In the future, we will extend the comparison of the kinematic parameters and joint mechanism to their optimization. Acceleration is not yet considered in the *performance index*, because its conversion to additional motor torque depends on the actuator and gear type as well as the gear ratio. It could be an important limit in high-geared motors. Furthermore, consideration of additional factors such as manipulability may be important for the design of humanoid robots. Next, we want to build a robot design assistant that aims to design real robots, taking into account the concrete physical properties of existing actuators to approach human motion in reality.

TABLE V: Power Requirement Index (PRI) and actuation power P[W] for different humanoid robot kinematics

	H		E		F		C	
	P	PRI	P	PRI	P	PRI	P	PRI
LIMS2	80	0.74	276	1.01	86	1.10	68	0.90
CENTAURO	155	1.43	480	1.76	175	2.24	116	1.54
iCub	99	0.91	381	1.40	78	0.99	92	1.21
David	111	1.02	322	1.18	93	1.19	71	0.94
HRP-4	84	0.78	340	1.25	77	0.98	78	1.03
Justin	77	0.71	268	0.99	76	0.98	67	0.88
Valkyrie	81	0.74	343	1.26	**67**	**0.85**	80	1.06
ARMAR-III	111	1.02	408	1.50	184	2.35	89	1.18
ARMAR-4	88	0.81	338	1.24	71	0.91	80	1.05
ARMAR-6	111	1.02	413	1.52	108	1.38	146	1.94
New Design	**63**	**0.58**	**198**	**0.73**	74	0.95	**60**	**0.79**
MMM	109	1.00	272	1.00	78	1.00	76	1.00

References

[1] T. Asfour, K. Regenstein, P. Azad, J. Schroder, A. Bierbaum, N. Vahrenkamp, and R. Dillmann, "Armar-III: An integrated humanoid platform for sensory-motor control," in *IEEE/RAS Intl. Conf. on Humanoid Robots (Humanoids)*. IEEE, 2006, pp. 169–175.

[2] T. Asfour, J. Schill, H. Peters, C. Klas, J. Bücker, C. Sander, S. Schulz, A. Kargov, T. Werner, and V. Bartenbach, "Armar-4: A 63 dof torque controlled humanoid robot," in *IEEE/RAS Intl. Conf. on Humanoid Robots (Humanoids)*. IEEE, 2013, pp. 390–396.

[3] T. Asfour, M. Waechter, L. Kaul, S. Rader, P. Weiner, S. Ottenhaus, R. Grimm, Y. Zhou, M. Grotz, and F. Paus, "Armar-6: A high-performance humanoid for human-robot collaboration in real-world scenarios," *IEEE Robotics & Automation Magazine*, vol. 26, no. 4, pp. 108–121, 2019.

[4] M. Grebenstein, A. Albu-Schäffer, T. Bahls, M. Chalon, O. Eiberger, W. Friedl, R. Gruber, S. Haddadin, U. Hagn, R. Haslinger, *et al.*, "The dlr hand arm system," in *IEEE Intl. Conf. on Robotics and Automation (ICRA)*. IEEE, 2011, pp. 3175–3182.

[5] C. Ott, M. A. Roa Garzon, F. Schmidt, W. Friedl, J. Englsberger, R. Burger, A. Werner, A. Dietrich, D. Leidner, B. Henze, *et al.*, "Mechanisms and design of dlr humanoid robots," *Humanoid Robotics: A Reference*, pp. 1–26, 2017.

[6] K. Kaneko, F. Kanehiro, M. Morisawa, K. Akachi, G. Miyamori, A. Hayashi, and N. Kanehira, "Humanoid robot hrp-4 - humanoid robotics platform with lightweight and slim body," *IEEE/RSJ Intl. Conf. on Intelligent Robots and Systems (IROS)*, pp. 4400–4407, 2011.

[7] N. A. Radford, P. Strawser, K. Hambuchen, J. S. Mehling, W. K. Verdeyen, A. S. Donnan, J. Holley, J. Sanchez, V. Nguyen, L. Bridgwater, *et al.*, "Valkyrie: Nasa's first bipedal humanoid robot," *Journal of Field Robotics*, vol. 32, no. 3, pp. 397–419, 2015.

[8] S. Kim, C. Kim, and J. H. Park, "Human-like arm motion generation for humanoid robots using motion capture database," in *IEEE/RSJ Intl. Conf. on Intelligent Robots and Systems (IROS)*. IEEE, 2006, pp. 3486–3491.

[9] K. E. Zelik and A. D. Kuo, "Human walking isn't all hard work: evidence of soft tissue contributions to energy dissipation and return," *Journal of Experimental Biology*, vol. 213, no. 24, pp. 4257–4264, 2010.

[10] C. Mandery, O. Terlemez, M. Do, N. Vahrenkamp, and T. Asfour, "Unifying representations and large-scale whole-body motion databases for studying human motion," *IEEE Transactions on Robotics*, vol. 32, no. 4, pp. 796–809, 2016.

[11] C. Mandery, Ö. Terlemez, M. Do, N. Vahrenkamp, and T. Asfour, "The kit whole-body human motion database," in *IEEE Intl. Conf. on Advanced Robotics (ICAR)*. IEEE, 2015, pp. 329–336.

[12] Y.-J. Kim, J.-I. Kim, and W. Jang, "Quaternion joint: Dexterous 3-dof joint representing quaternion motion for high-speed safe interaction," in *IEEE/RSJ Intl. Conf. on Intelligent Robots and Systems (IROS)*. IEEE, 2018, pp. 935–942.

[13] C. Klas and T. Asfour, "A compact, lightweight and singularity-free wrist joint mechanism for humanoid robots," in *IEEE/RSJ Intl. Conf. on Intelligent Robots and Systems (IROS)*, 2022, pp. 457–464.

[14] W. Xu, X. Li, W. Xu, L. Gong, Y. Huang, Z. Zhao, L. Zhao, B. Chen, H. Yang, L. Cao, *et al.*, "Human-robot interaction oriented human-in-the-loop real-time motion imitation on a humanoid tri-co robot," in *International Conference on Advanced Robotics and Mechatronics (ICARM)*. IEEE, 2018, pp. 781–786.

[15] N. Jaquier, L. Rozo, and S. Calinon, "Analysis and transfer of human movement manipulability in industry-like activities," in *IEEE/RSJ Intl. Conf. on Intelligent Robots and Systems (IROS)*. IEEE, 2020, pp. 11 131–11 138.

[16] A. Di Fava, K. Bouyarmane, K. Chappellet, E. Ruffaldi, and A. Kheddar, "Multi-contact motion retargeting from human to humanoid robot," in *IEEE/RAS Intl. Conf. on Humanoid Robots (Humanoids)*. IEEE, 2016, pp. 1081–1086.

[17] K. Aberman, P. Li, D. Lischinski, O. Sorkine-Hornung, D. Cohen-Or, and B. Chen, "Skeleton-aware networks for deep motion retargeting," *ACM Transactions on Graphics (TOG)*, vol. 39, no. 4, 2020.

[18] T. Kim and J.-H. Lee, "C-3po: Cyclic-three-phase optimization for human-robot motion retargeting based on reinforcement learning," in *IEEE Intl. Conf. on Robotics and Automation (ICRA)*. IEEE, 2020, pp. 8425–8432.

[19] J. Lim, H. J. Chang, and J. Y. Choi, "Pmnet: Learning of disentangled pose and movement for unsupervised motion retargeting." in *British Machine Vision Conference (BMVC)*, 2019.

[20] S. Arimoto and M. Sekimoto, "Human-like movements of robotic arms with redundant DOFs: virtual spring-damper hypothesis to tackle the Bernstein problem," in *IEEE Intl. Conf. on Robotics and Automation (ICRA)*, May 2006, pp. 1860–1866.

[21] P. Zhang, Z. Yao, and Z. Du, "Global Performance Index System for Kinematic Optimization of Robotic Mechanism," *Journal of Mechanical Design*, vol. 136, no. 3, p. 031001, 12 2013.

[22] N. Vahrenkamp, T. Asfour, and R. Dillmann, "Robot placement based on reachability inversion," in *IEEE Intl. Conf. on Robotics and Automation (ICRA)*. IEEE, 2013, pp. 1970–1975.

[23] T. Yoshikawa, "Manipulability of robotic mechanisms," *The international journal of Robotics Research*, vol. 4, no. 2, pp. 3–9, 1985.

[24] N. Vahrenkamp, T. Asfour, G. Metta, G. Sandini, and R. Dillmann, "Manipulability analysis," in *IEEE/RAS Intl. Conf. on Humanoid Robots (Humanoids)*. IEEE, 2012, pp. 568–573.

[25] J.-O. Kim and K. Khosla, "Dexterity measures for design and control of manipulators," in *IEEE/RSJ International Workshop on Intelligent Robots and Systems*. IEEE, 1991, pp. 758–763.

[26] H. Wang, S. Fan, and H. Liu, "An anthropomorphic design guideline for the thumb of the dexterous hand," in *IEEE International Conference on Mechatronics and Automation*. IEEE, 2012, pp. 777–782.

[27] B.-H. Jun, P.-M. Lee, and J. Lee, "Manipulability analysis of underwater robotic arms on rov and application to task-oriented joint configuration," in *Oceans' 04 MTS/IEEE Techno-Ocean'04 (IEEE Cat. No. 04CH37600)*, vol. 3. IEEE, 2004, pp. 1548–1553.

[28] N. Jaquier, L. Rozo, D. G. Caldwell, and S. Calinon, "Geometry-aware manipulability learning, tracking, and transfer," *The International Journal of Robotics Research*, vol. 40, no. 2-3, pp. 624–650, 2021.

[29] N. Cheney, R. MacCurdy, J. Clune, and H. Lipson, "Unshackling evolution: evolving soft robots with multiple materials and a powerful generative encoding," *ACM SIGEVOlution*, vol. 7, no. 1, pp. 11–23, 2014.

[30] A. Meixner, C. Hazard, and N. Pollard, "Automated design of simple and robust manipulators for dexterous in-hand manipulation tasks using evolutionary strategies," in *IEEE/RAS Intl. Conf. on Humanoid Robots (Humanoids)*, 2019, pp. 281–288.

[31] N. Bredeche and J.-M. Montanier, "Environment-driven embodied evolution in a population of autonomous agents," in *International Conference on Parallel Problem Solving from Nature*. Springer, 2010, pp. 290–299.

[32] M. V. Liarokapis, P. Artemiadis, C. P. Bechlioulis, and K. J. Kyriakopoulos, "Directions, methods and metrics for mapping human to robot motion with functional anthropomorphism: A review," *School of Mechanical Engineering, National Technical University of Athens, Tech. Rep*, 2013.

[33] M. J. Gielniak, C. K. Liu, and A. L. Thomaz, "Generating human-like motion for robots," *The International journal of robotics research*, vol. 32, no. 11, pp. 1275–1301, 2013.

[34] F. Zacharias, C. Schlette, F. Schmidt, C. Borst, J. Rossmann, and G. Hirzinger, "Making planned paths look more human-like in humanoid robot manipulation planning," in *IEEE Intl. Conf. on Robotics and Automation (ICRA)*. IEEE, 2011, pp. 1192–1198.

[35] E. Buckingham, "On physically similar systems; illustrations of the use of dimensional equations," *Physical review*, vol. 4, no. 4, p. 345, 1914.

[36] H. Song, Y.-S. Kim, J. Yoon, S.-H. Yun, J. Seo, and Y.-J. Kim, "Development of low-inertia high-stiffness manipulator lims2 for high-speed manipulation of foldable objects," in *IEEE/RSJ Intl. Conf. on Intelligent Robots and Systems (IROS)*. IEEE, 2018, pp. 4145–4151.

[37] N. Kashiri, L. Baccelliere, L. Muratore, A. Laurenzi, Z. Ren, E. M. Hoffman, M. Kamedula, G. F. Rigano, J. Malzahn, S. Cordasco, *et al.*, "Centauro: A hybrid locomotion and high power resilient manipulation platform," *IEEE Robotics and Automation Letters*, vol. 4, no. 2, pp. 1595–1602, 2019.

[38] N. G. Tsagarakis, G. Metta, G. Sandini, D. Vernon, R. Beira, F. Becchi, L. Righetti, J. Santos-Victor, A. J. Ijspeert, M. C. Carrozza, *et al.*, "icub: the design and realization of an open humanoid platform for cognitive and neuroscience research," *Advanced Robotics*, vol. 21, no. 10, pp. 1151–1175, 2007.

[39] D. Shah, Y. Wu, A. Scalzo, G. Metta, and A. Parmiggiani, "A comparison of robot wrist implementations for the icub humanoid," *Robotics*, vol. 8, no. 1, p. 11, 2019.